Global Change Biology

Global Change Biology (2010) **16**, 1213–1228, doi: 10.1111/j.1365-2486.2009.02094.x

Greenhouse gas, upwelling-favorable winds, and the future of coastal ocean upwelling ecosystems

ANDREW BAKUN*, DAVID B. FIELD†, ANA REDONDO-RODRIGUEZ‡ and SCARLA J. WEEKS‡

*Rosenstiel School of Marine and Atmospheric Science, University of Miami, Miami, FL 33149, USA, †College of Natural Sciences, Hawaii Pacific University, Kaneohe, HI 96744, USA, ‡Centre for Marine Studies, University of Queensland, Brisbane, Qld 4072, Australia

Abstract

Coastal ocean upwelling ecosystems generally represent the most productive large marine ecosystems of the world's oceans, in terms of both primary production rates and tonnages of exploitable fish produced. The Peruvian upwelling system, in particular, stands out as a major factor in world fish production. The Pacific trade winds have traditionally been considered to be the primary driving force for the upwelling system off Peru, but are projected to weaken as climate change proceeds. This leads to concern that the upwelling process in the Peru system, to which its productivity is linked, may likewise weaken. However, other mechanisms involving greenhouse-associated intensification of thermal low-pressure cells over the coastal landmasses of upwelling regions suggest general intensification of wind-driven ocean upwelling in coastal upwelling regions of the world's oceans. But although certain empirical results have supported this expectation, it has not been consistently corroborated in climate model simulations, possibly because the scale of the coastal intensification may be small relative to the scales that are appropriately reflected in the standard models. Here we summarize available evidence for the intensification mechanism and present a proxy test that uses variations in water vapor, the dominant natural greenhouse gas, to offer multiple-realization empirical evidence for action of the proposed mechanism in the real world situation. While many potential consequences to the future of marine ecosystems would codepend on climate change-related changes in the thermocline and nutricline structures, an important subset, involving potential increased propensities for hypoxia, noxious gas eruptions, toxic red tide blooms, and/or jellyfish outbreaks, may depend more directly on changes in the upwelling-favorable wind itself. A prospective role of fisheries in either mitigating or reinforcing this particular class of effects is suggested.

Keywords: climate change, ecosystem regime shift, ENSO, greenhouse gas, hypoxia, jellyfish outbreaks, sardines, upwelling intensification

Received 19 April 2009; revised version received 8 September 2009 and accepted 9 September 2009

Introduction

U*pwelling* zones arranged along the temperate eastern boundaries of the Pacific and Atlantic Oceans are among the most productive regions of the world's oceans. They are defined by the characteristic wind patterns that push surface waters offshore and thus pump (i.e., 'upwell') nutrient-rich deeper waters into the illuminated surface layers where they are available to support photosynthesis. These zones are characterized by massive populations of small pelagic fishes such as sardines and anchovies, and support large populations of seabirds and marine mammals as well as important coastal fisheries.

For example, in the late 1960s the single country, Peru, exploiting a single fish species, the Peruvian anchoveta (*Engraulis ringens*), produced more total tonnage of fish than the grand total of all the other fish species, both marine and freshwater, exploited by all the other countries of North and South America combined. This unique capacity of the Peruvian upwelling ecosystem to produce huge quantities of fish continues to render it a major factor in overall world fish production. The upwelling-favorable winds that drive the Peruvian system separate from the South American coast immediately after exiting the coastal upwelling zone, thereupon merging directly into the Pacific southeast trade

Correspondence: Andrew Bakun, tel. +1 305 421 4986, fax +1 305 421 4600, e-mail: abakun@rsmas.miami.edu

wind system. Consequently, the Peruvian upwelling is traditionally described as being driven directly by the Pacific trade winds (Paulik, 1971). While different analyses of the 20th century data give conflicting results (Cane *et al.*, 1997; Vecchi *et al.*, 2006), a recent analysis of climate model simulations has concluded that the trade winds in the equatorial Pacific have weakened in response to the progressive build up of atmospheric greenhouse gases (Vecchi *et al.*, 2006). Accordingly, there is concern that the Peruvian coastal upwelling system may weaken in the future.

Opposing this particular concern are earlier premises (Bakun, 1990; Diffenbaugh *et al.*, 2004) that predict intensification of coastal upwelling in major upwelling zones of the world as atmospheric greenhouse gas concentrations increase. Moreover, corroboration of this prediction appears to be unfolding as credible paleosedimentary studies accrue (Otto-Bliesner *et al.*, 2003; McGregor *et al.*, 2007; Gutiérrez *et al.*, 2009) and historical time series of recorded observations continue to lengthen (Bakun, 1992; Schwing & Mendelssohn, 1997). However, climate model simulations have not provided consistent corroboration (Wang *et al.*, 2009), which has tended to block credence in the intensification prognosis.

Intensification mechanism

Throughout the world's oceans, coastal upwelling tends to operate predominately during the 'heating portions' of the year (spring and summer in subtropical latitudes, year-round in tropical latitudes) when, because of the much greater heat storage capacity of ocean waters compared with land surfaces, air temperature over a coastal landmass tends to increase relative to that over the adjacent sea. This causes a strong pressure gradient to form between a thermal low-pressure cell that develops over the heated land surface and the higher pressure existing over the cooler ocean (Fig. 1a). This cross-shore pressure gradient supports an alongshore geostrophic wind that drives an offshore-directed Ekman transport of surface waters. When the surface waters are thereby forced offshore from the solid coastal boundary on spatial scales too large for

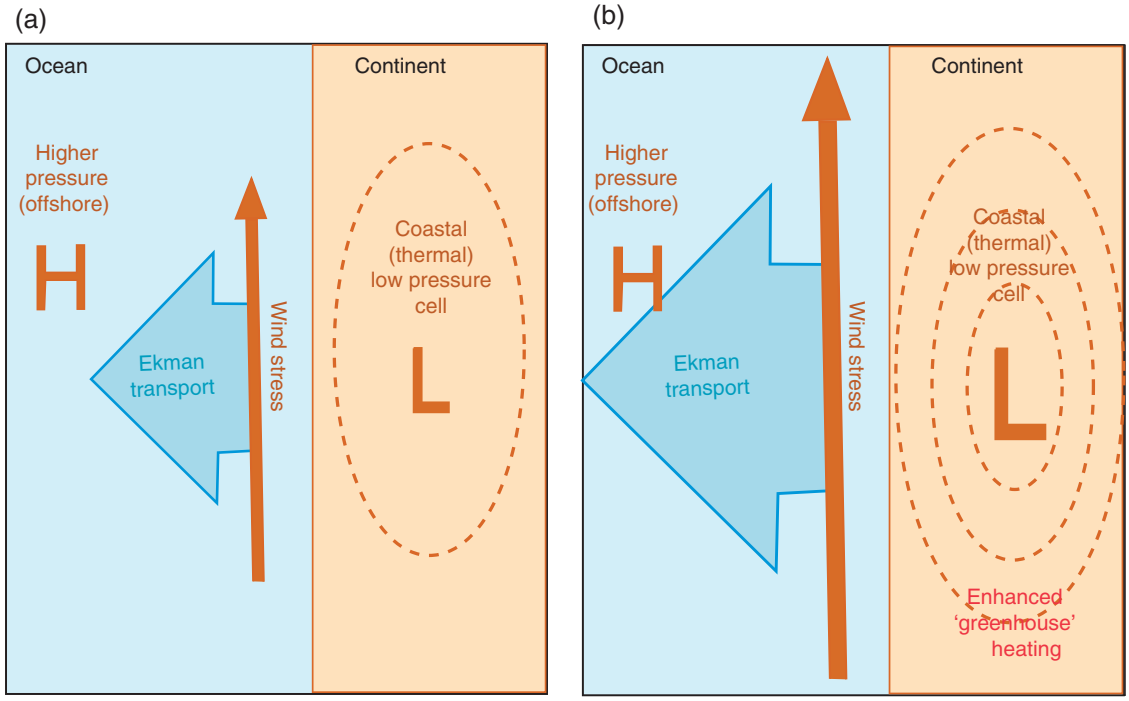

Fig. 1 Diagram of the upwelling intensification mechanism: (a) a 'thermal' low-pressure cell builds up over the coastal landmass due to heating of the continental surface relative to the more slowly heating ocean, exerting equatorward geostrophic wind stress on the sea surface that, in turn, drives offshore-directed Ekman transport of ocean surface water and corresponding upwelling of deeper waters required to replace the surface waters transported offshore; (b) buildup of greenhouse gases in the atmosphere inhibits nighttime cooling of the heated coastlands, increasing average intensity of the coastal low-pressure cell and associated upwelling-favorable wind, which in terms drives increases in offshore surface transport and in resulting upwelling. (A southern hemisphere configuration is depicted in this figure. The upwelling-favorable wind blows equatorward along an eastern ocean continental in either hemisphere; accordingly for a northern hemisphere version of this figure, one would simply reverse the direction of the wind stress vector symbol while keeping all other aspects unchanged.)

them to be replaced by waters moving horizontally along the coast, mass balance is maintained by upwelling of subsurface waters (Sverdrup, 1938; Wooster & Reid, 1963). In the case of Peru, the low latitude situation results in upwelling-favorable winds year round, with a wintertime strengthening of the anticyclonic subtropical high offshore producing a seasonal strengthening of the pressure gradient.

Eastern sides of oceans are characterized by much drier atmospheres than are their western sides. Because the most important greenhouse gas in the earth's atmosphere is water vapor (Houghton, 2001), eastern ocean boundary regions tend innately to experience a reduced natural greenhouse effect. Consequently, local cooling by long wave radiation is rapid and efficient. This facilitates the relaxation of the thermal low-pressure cells that build up over the coastal landmass due to daytime heating.

However, as anthropogenic greenhouse gas concentrations increase in the atmosphere, radiative cooling will be increasingly suppressed, particularly because the associated increases in air temperature will allow ever greater concentrations of water vapor to be maintained in the lower atmosphere thereby multiplying the effects of the anthropogenically added gases. As a result, the rate of heating over the land will be further enhanced relative to that over the ocean, causing further intensification of the low-pressure cell over the coastal landmass. The resulting pressure gradient increase is matched by a proportional wind increase, which causes a nonlinear (quadratic or greater) increase in intensity of resulting upwelling (Fig. 1b). Moreover, additional potentially contributing mechanisms altering the intensity of thermal low-pressure cell over the coastlands could involve greenhouse-associated effects that reduce the vegetation cover on the land surface (Diffenbaugh *et al*., 2004), thereby lessening its cooling effect, as well as alterations in incidence of coastal fog and low-level stratus clouds that could affect landmass heating (Enfield, 1981; Vargas *et al*., 2007). Unfortunately, the persistent marine stratus clouds that characterize upwelling zones are often poorly simulated in climate models (e.g., Boville & Gent, 1998).

Earlier empirical evidence

An obvious approach to verifying the real-world operation of these mechanisms is the one adopted by Bakun (1990), i.e., simply assembling long time series of wind data collected in these upwelling zones during the period of progressive buildup of greenhouse gases, and demonstrating a global pattern of upward trends in wind intensity in the direction favorable for upwelling.

A number of additional corroborative examples have appeared more recently. A long-term increasing trend in upwelling-favorable wind intensity is clearly evident in maritime data summaries off Peru (e.g., Bakun & Weeks, 2008; see also the newly assembled 'Peru–τ' series displayed in Fig. 2 of this paper). Santos *et al*. (2005) reported a similar increasing trend in the upwelling region off NW Africa. Shannon *et al*. (1992) reported a long-term increase in upwelling-favorable wind off South Africa. Mendelssohn & Schwing (2002) showed increasing long-term wind trends in the California upwelling zone. Di Lorenzo *et al*. (2005) also detected a trend in upwelling favorable winds (yet interestingly found that higher SSTs accompanied the increased wind strength as a result of greater large-scale ocean–atmosphere heat exchange, thereby underscoring the fact that SSTs are not necessarily indicative of upwelling strength).

But a vexing problem intrudes to confuse clear interpretation of these data. Inconveniently, there appears to be a likelihood that a completely artificial long-term increasing trend may generally contaminate any wind intensity time series derived from maritime wind reports (Ramage, 1987; Cardone *et al*., 1990). There appear to be several potential sources of this artifact, including temporal trends in ship sizes and associated anemometer heights, trends in relative frequencies of measured and estimated (Beaufort scale, etc.) winds, and nonhomogeneities in recording and archiving practices. Bakun (1992) separately analyzed measured and estimated maritime wind reports in the particularly data-rich upwelling zone off the Iberian Peninsula and concluded that there was evidence for both sources of increasing wind trends, the artificial one and the real one, occurring simultaneously in upwelling zones. Unfortunately, both being simple long-term trends, separating their respective roles in the overall series trend is difficult. As a result, one cannot confidently decide whether the evident long-term increasing trend in the upwelling-favorable wind stress off Peru (Fig. 2) might represent a real long-term intensification that might be reasonably attributed to atmospheric greenhouse gas buildup via the mechanism depicted in Fig. 1, or rather, merely be a result of the proposed artifact. (A 'proxy test' highlighted later in this paper represents one sort of attempt to circumvent the problem of lack of sufficient realizations of the process to infer causality.)

Another approach to attempting to isolate one factor from the other is to make use of evident spatial patterns on the basis that the artifact should be dependent only on wind speed itself while the real trend should be linked to thermal coastal low development. Bakun (1992) tracked spatial variations of long-term wind trends around the periphery of the North Atlantic

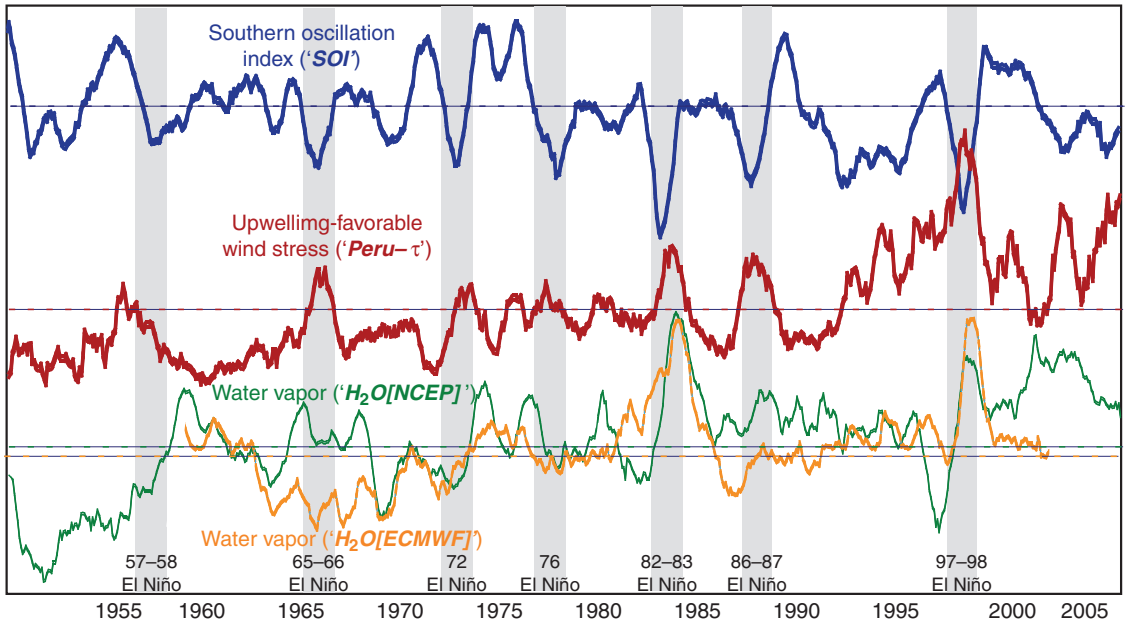

Fig. 2 Low passed time series (12-month running means) of monthly values of the Southern Oscillation Index (SOI), upwelling-favorable wind stress off Peru, and of 'precipitable water' (or 'total water column water vapor') from the National Centre for Environmental Prediction (NCEP) and European Centre for Medium-range Weather Forecasts (ECMWF) reanalysis data sets, at a grid location near the Peru coast (10°S, 80°W). Gray vertical bars identify time periods of substantial El Niño episodes.

subtropical gyre, and found a consistent pattern of increasing wind trends in locations subject to formation of coastal thermal lows during the spring-summer heating portions of the year. Conversely, locations remote from any adjacent seasonally heated landmass exhibited generally decreasing wind trends. Similarly, Schwing & Mendelssohn (1997) and Mendelssohn & Schwing (2002) showed that the indicated long-term increase in upwelling favorable wind off California was largely confined to the main upwelling zone itself, i.e., to the stretch of coast, as well as to the seasonal period, characterized by thermal low-pressure cell development; they found that the increase tended to vanish or reverse elsewhere. A different approach is to seek corroboration in a completely different type of observational data. For example, a long-term increase in upwelling-producing wind stress should be reflected in a corresponding increase in alongshore slope in mean sea level (Csanady, 1978; Enfield & Allen, 1980; Bigg & Gill, 1986). Accordingly, independent corroboration of the apparent long-term increasing trends in upwelling-favorable wind intensity has been sought, with a certain degree of success, in independent sea level time series, both off Peru (Bigg, 1988) and off the Iberian Peninsula (Bakun, 1992).

Using proxy temperature data derived from sedimentary records, McGregor *et al*. (2007) inferred an increase in coastal upwelling off NW Africa during the 20th Century from proxy temperatures based on the alkenones of coccolithophorids. Although changes in the vertical distribution of coccolithophorids or their seasonal cycle could affect the inferred temperature decrease, Van Geen *et al*. (1992) found evidence of higher upwelling 4000 years ago in the California Current, when northern hemisphere insolation was higher, which would support a link between the continental heating with a greater land–sea temperature gradient, and upwelling winds.

Indications from climate change models

Shortly after Bakun's (1990) introduction of the upwelling intensification prognosis, Hsieh & Boer (1992) searched for corroboration in a climate model simulation running at a grid resolution of 300–400 km. But rather than the predicted intensification, this model predicted a general pattern of weakened upwelling in the major eastern ocean boundary upwelling zones, recalling a common pattern in early climate change simulation models (e.g., Manabe & Weatherald, 1980) of general relaxation of the large-scale subtropical oceanic and atmospheric gyral circulations as atmospheric greenhouse gas concentrations build up. Somewhat more recently, Mote & Mantua (2002) examined outputs of two later-generation, smaller scale (~ 200 km grid resolution) models and found that, while not

demonstrating actual intensification, they did not replicate the earlier indication of weakened upwelling. Shortly afterward, Snyder *et al*. (2003) implemented a much finer scale ($\sim$ 40 km grid resolution) 'regional' model for the California system and found a definite intensification of the upwelling season. More recent fine-scale modeling work by the same group continues to support a prognosis for strong increase in upwelling favorable winds off California (e.g., UCSD, 2008).

Thus, it appears that rather than contradictory results among different model studies, it may simply be an issue of scale dependence. In the earlier larger-scale simulations, the basic computation grid mesh spanned hundreds of km between data points, with results necessarily smoothed over multiple grid intersections at each computation step. Thus the smaller coastal scales on which actual intensification may occur, which extend to the scales on which the local diurnal sea breeze – land breeze mechanisms act (i.e., tens of kilometers or less), may have been effectively swamped by the larger basin-scale relaxation tendency and totally obscured in the integrated result. It is only when the scale of the basic computations is reduced to the scale at which the intensification mechanism (Fig. 1) actually acts, that the mechanistic models can produce the resulting effect. It should be noted that the common practice of hydrodynamic or statistical *downscaling* of results from a large-scale model simulation cannot generate a valid characterization of a smaller-scale effect that was not appropriately incorporated in the dynamics of the large-scale simulation itself (e.g., von Storch *et al*., 2000; Rockel *et al*., 2008).

A new 'proxy' test

A major element of the development of an El Niño episode is the collapse of the Pacific Walker Circulation and a resulting drastic weakening of the Pacific equatorial trade winds (Bjerknes, 1966; Wyrtki, 1975). The coastwise winds off Peru, upon exiting the coastal upwelling zone, merge directly into this trade wind flow. However, the wind stress that drives upwelling in that zone tends to increase (Fig. 2), rather than decrease, during an El Niño event (Wyrtki, 1975; Enfield, 1981; Bakun & Weeks, 2008). Enfield (1981) suggested that decreased cloudiness over the Peruvian coastlands during El Niño episodes, by permitting greater heating of the land surface within the coastal thermal low-pressure cell (Fig. 1b), might be the primary causative factor. Perhaps offering some degree of argument against a primary mechanism based on decreased cloudiness, i.e., on less atmospheric water vapor condensation, or working in conjunction with this mechanism, is the fact that collapse of the Walker Circulation during an El Niño event radically increases the water vapor content in the atmosphere of the eastern side of the Pacific (Fig. 3d and e).

Bakun & Weeks (2008) put forth an explanation based on the more direct greenhouse-gas-related mechanism proposed by Bakun (1990), their reasoning being as follows. The most important greenhouse gas in the earth's atmosphere is water vapor (Houghton, 2001). This acts to enhance the local 'greenhouse heating' effect and, correspondingly, the strength of the thermal low-pressure cell over coastal landmasses (Fig. 1). This in turn supports intensification of the upwelling-favorable alongshore geostrophic wind even as the trade winds, into which it directly feeds, slacken. (Obviously, mass continuity must be preserved, and so the airflow evidently must broaden in some manner as it lessens in velocity).

Bakun & Weeks (2008) displayed a series of earlier published wind stress data extending only up to 1987. For the present study we have used an entirely newly constructed time series (Fig. 2) that extends to more recent years (to 2005), and have also gathered other relevant time series, notably estimates of atmospheric water vapor, to try to develop a more direct empirical linkage and to perhaps as well gain some insight into the relative effects of the Bakun (1990) greenhouse gas mechanism and the Enfield (1981) cloudiness mechanism. The greater realizations of the ENSO cycle provide a means to test the consistency of the relationship between increases in coastal upwelling winds with continental warming associated with greater greenhouse gas concentrations.

Materials and methods

A monthly time series of upwelling favorable wind stress off Peru (Peru–τ) (Figs 2 and 3, Tables 1 and 2) was produced from ship observations extracted from the International Comprehensive Ocean–Atmosphere Data Set (ICOADS). Wind stress was calculated for each individual observation by converting wind speed into eastward (u) and northward (v) velocity components. Eastward and northward wind stress components were calculated, respectively, as $1.22\, C_D\, u \sqrt{u^2+v^2}$ and $1.22\, C_D\, v \sqrt{u^2+v^2}$ using the drag coefficient (C_D) formulation of Yelland and Taylor (1996). The alongshore (upwelling favorable) windstress was then calculated by resolving the component of the calculated stress vectors in the (equatorward) alongshore direction. The monthly average was calculated from all windstress observations between 7 and 14°S and east of 280°. Optimum interpolation (OI) sea surface temperature data (Fig. 3), available at 1° grid resolution from 1982 to present, were downloaded from the NOAA OI SST

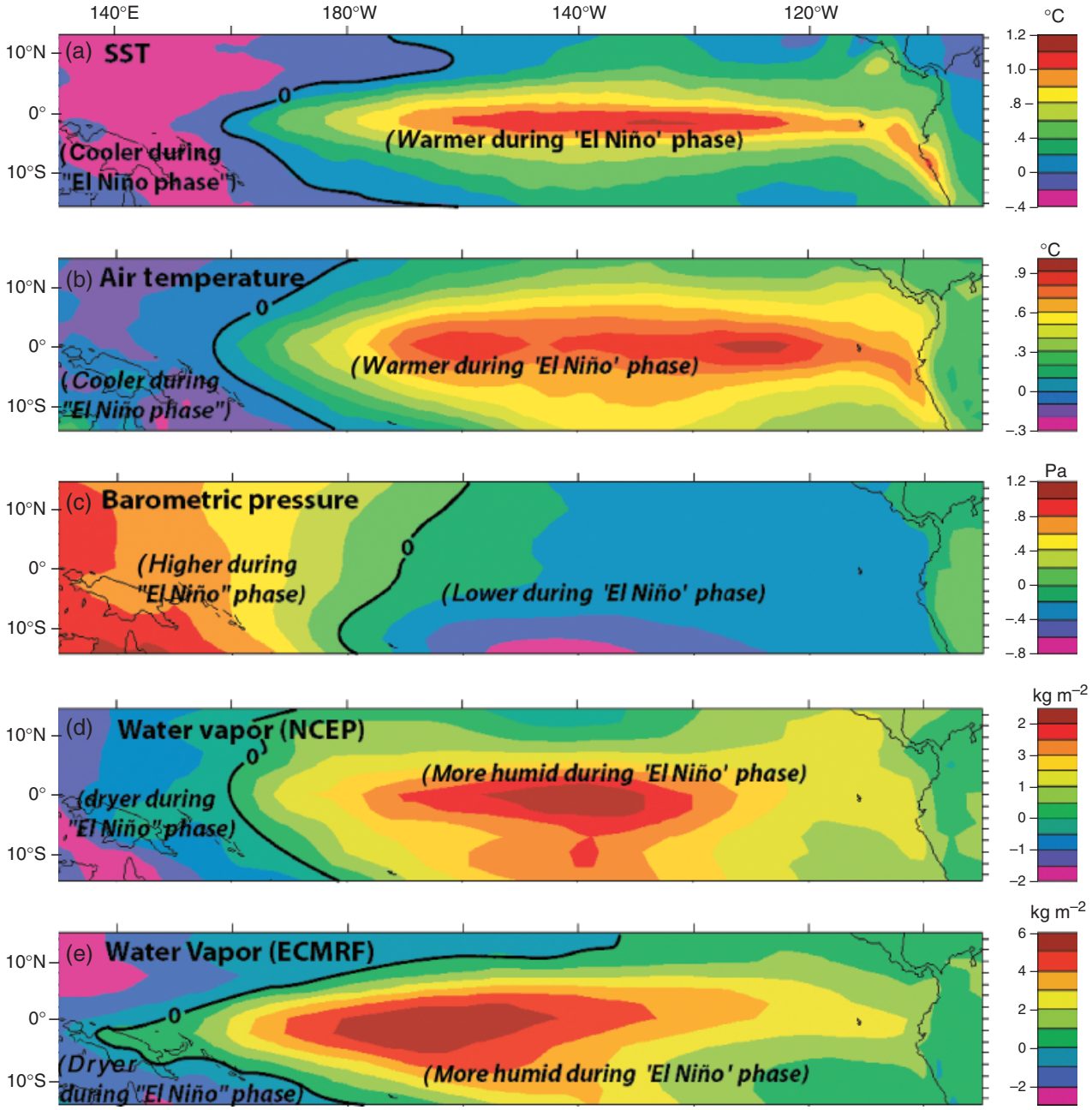

Fig. 3 Distributions of the slopes of linear regressions (calculated at 2.5° latitude–longitude grid intersections along an equatorial strip of the Pacific Ocean between 12.5°N and 12.5°S latitudes) of time series of October through March means (intended to characterize the 'heating' portion of the year in the southern hemisphere) of the Southern Oscillation Index against corresponding time series of (a) sea surface temperature, (b) near-surface air temperature, (c) sea level atmospheric pressure, and 'total column water vapor' (or 'precipitable water') from the (d) National Centre for Environmental Prediction (NCEP) and (e) European Centre for Medium-range Weather Forecasts (ECMWF) reanalysis projects.

V1 data site, (http://www.cdc.noaa.gov/cdc/data.noaa.oisst.v2.html). Monthly time series of sea level pressure and air temperature (Fig. 3), available at a resolution of 2.5°, for the period 1948 to present were sourced from the National Centre for Environmental Prediction/National Centre for Atmospheric Research (NCEP/NCAR) 40-year Reanalysis Project (http://www.cdc.noaa.gov/cdc/data.ncep.reanalysis.html). Monthly time series of atmospheric water vapor content (Figs 2, 3 and 5; Tables 1 and 2) were obtained from two sources: (1) monthly time series of 'precipitable water' for the period 1948 to present were sourced from the

Table 1 Correlation coefficients (r) between respective pairs of annual-mean and quarterly-mean time series of monthly values of: upwelling-favorable wind stress off Peru (*Peru*–$\overrightarrow{\tau}$), Southern Oscillation Index (SOI), and the two available reconstructions of water vapor concentration (H_2O [NCEP] and H_2O [ECMWF]) at a point near the Peru coast

	Annual mean	*1st QTR*	*2nd QTR*	*3rd QTR*	*4th QTR*	*Composite P*
(*a*) *Water vapor: *[NCEP] vs. [ECMWF]* (*44 years – 1958–2001*)						
Raw	0.50$^{***\&}$	0.44$^{***\&}$	0.75$^{***\&\&\&}$	0.62***	0.33*	$\ll$ 0.000001
Δ*ENSO*	0.47***	0.39**	0.75$^{***\&\&\&}$	0.60$^{***\&}$	0.28*	$\ll$ 0.000001
1st-diff. (raw)	0.62$^{***\&\&\&}$	0.56$^{***\&\&\&}$	0.77$^{***\&\&\&}$	0.51$^{***\&\&}$	0.51$^{***\&\&}$	0.000001
(*b*) *Water vapor [NCEP] vs. SOI* (*56 years – 1950–2005*)						
Raw	–0.27*	–0.28*	–0.17	–0.25*	–0.26*	< 0.0008
1st-diff. (raw)	–0.23*	–0.42$^{***\&}$	–0.**12**	–0.19	–0.27*	< 0.00003
(*c*) *Water vapor [ECMWF] vs. SOI* (*44 years – 1958–2001*)						
Raw	–0.29*	–0.31*	–0.21	–0.17	–0.26*	< 0.002
1st-diff. (raw)	–0.29*	–0.50$^{***\&\&}$	–0.14	–0.20	–0.30$^{*\&}$	< 0.000005
(*d*) *Peru*–$\overrightarrow{\tau}$ *vs. SOI* (*56 years – 1950–2005*)						
Raw	–0.35**	–0.53$^{***\&}$	–0.33**	–0.12	–0.20*	< 0.00005
1st-diff. (raw)	–0.35$^{**\&}$	–0.66$^{***\&\&\&}$	–0.20	–0.03	–0.24*	< 0.0000002
(*e*) *Peru*–$\overrightarrow{\tau}$*vs. water vapor* (*NCEP*) (*56 years – 1950–2005*)						
Raw	0.46$^{***\&\&}$	0.23*	0.46$^{***\&}$	0.47$^{**\&}$	0.30*	< 0.00004
Δ*ENSO*	0.41***	0.09	0.43$^{***\&}$	0.46$^{***\&}$	0.27*	< 0.0003
1st-diff. (raw)	0.30$^{*\&}$	0.17	0.29*	0.15	0.23*	< 0.0002
(*f*) *Peru*–$\overrightarrow{\tau}$ *vs. water vapor [ECMWF]* (*44 years – 1958–2001*)						
Raw	0.48$^{***\&}$	0.27*	0.53$^{***\&\&\&}$	0.42***	0.42$^{***\&}$	< 0.00003
Δ*ENSO*	0.44**	0.13	0.50$^{***\&}$	0.41**	0.39$^{**\&}$	< 0.00003
1st-diff. (raw)	0.43$^{**\&}$	0.42$^{**\&}$	0.44$^{**\&\&}$	0.14	0.46$^{**\&\&}$	$\ll$ 0.000001

Significance levels assuming annual values represent independent degrees of freedom): $^{*}P<0.05$, $^{**}P<0.01$, $^{***}P<0.001$.
(Because the mechanism being addressed demands a given sign for each correlation, we consider a 'one-tailed' tests to be appropriate here.)
Significance levels assuming df is the smaller value in each respective series pair of zero crossings shown in Table 2: $^{\&}P<0.05$, $^{\&\&}P<0.01$, $^{\&\&\&}P<0.001$.
The rightmost column (labeled '*Composite P*'') lists the probability of finding an equivalent sequence of similarly signed correlations among independent seasonal series pairs based on the '& – symbol' criterion (see text).
ECMWF, European Centre for Medium-range Weather Forecasts; NCEP, National Centre for Environmental Prediction; 1st diff., first difference.

NCEP/NCAR Reanalysis Project (see previous sentence) and (2) monthly time series of 'total column water vapor' for the period September 1957 to August 2002 were obtained from the European Centre for Medium-range Weather Forecasts (ECMWF) ERA_40 Reanalysis Project (http://www.ecmwf.int/research/era/). Southern Oscillation Index (SOI) data used in Figs 2 and 4 and Tables 1 and 2) were obtained from the Climatic Research Unit, University of East Anglia, UK (http://www.cru.uea.ac.uk/cru/data/soi.htm).

In order to show the response of the variables (water vapor, air temperature, SST, and sea level barometric pressure) to the ENSO signal (Figs 3 and 4), the slopes of the linear regressions between the SOI and each variable were calculated and the corresponding plots generated. The monthly mean values were reduced to a single value per year corresponding to the mean from October to March, designed to characterize the 'heating' portion of the year in the southern hemisphere. Using NOAA's FERRET Program (a product of NOAA's Pacific Marine Environmental Laboratory: http://

Table 2 Number of 'crossings of the mean', assumed to represent a minimal estimate of available empirical degrees of freedom, in each of data series analyzed

	Annual mean	1st QTR	2nd QTR	3rd QTR	4th QTR
SOI					
Raw	23	25	27	29	24
1st-diff. (raw)	33	30	29	37	35
Upwelling favorable wind stress off Peru (*Peru*–$\vec{\tau}$)					
Raw	15	19	21	16	19
Δ*ENSO*	19	17	22	19	21
1st-diff. (raw)	32	32	35	35	41
Water vapor (*NCEP*)					
Raw	15	14	19	14	27
Δ*ENSO*	17	15	20	17	25
1st-diff. (raw)	34	36	31	33	37
Water vapor (*ECMWF*)					
Raw	14	12	15	8	24
Δ*ENSO*	11	16	20	10	19
1st-diff. (raw)	28	29	30	27	30

The smaller of the respective two values for each of the series pairs analyzed is assumed to represent the available degrees of freedom for the "'&' – criterion" significance estimates cited in Table 1 and in the text.
ECMWF, European Centre for Medium-range Weather Forecasts; NCEP, National Centre for Environmental Prediction; SOI, Southern Oscillation Index; 1st diff., first difference.

www.ferret.noaa.gov), linear regressions between the SOI mean values and the various other data types shown were calculated for each available grid point within the areas shown.

Issues of time series homogeneity, validity and empirical degrees of freedom

Forming homogeneous, coherent multidecadal environmental data series presents notable problems. Even if a consistent measurement may be taken at a consistent location, it seldom represents a homogeneous time series over multidecadal periods due to a number of factors that include wear on the sensor system, changes in the very local area near the sensor that affect the measurement, etc. Moreover, real small-spatial-scale variability may render any 'point' measurement nonrepresentative of the larger scale of interest that it may be intended to characterize. Accordingly, one hopes to minimize such issues by blending data from a number of sources and locations via an objective analysis procedure (Gandin, 1965; Ludwig & Sinton, 2000). The global data analyses on which we depend for this study (see previous section) are necessarily produced on fairly large-mesh analysis grids that spread data over substantial spatial scales. In the Peruvian case, data over the ocean area are available mostly at sea level, while those immediately inland are from high altitude locations on the slopes of the Andes Mountain range, with no way to accurately extrapolate these downward through the solid earth to a consistent sea level reference. Data at much lower altitudes may be found further inland in the Amazon Valley, but conditions there are isolated from the conditions at the coast by an unbroken barrier of high mountains. Evidence of this problem can be seen in Fig. 4 where pressure and water vapor anomaly distributions exhibit quite abrupt discontinuities at the South American coast. In such zones of topographic discontinuity, objective analysis of spatially spread data is clearly problematic.

An additional feature of the various data series produced for this study is a substantial degree of long-period behavior that undoubtedly results from a combination of several factors including (1) quasi-random 'red noise' climatic variability, (2) a particularly large component of cyclic interannual ENSO-scale variability characteristic of the region, and probably (3) spurious low-frequency features and trends introduced by secular changes in data densities and distribution and by nonhomogeneities in analysis and in measurement techniques and instrumentation. The resulting autocorrelation presents issues regarding the degrees of freedom available for the statistical tests reported here. Of course, seasonality needs to be removed to avoid artificial inflation of apparent significance levels; we accomplish this by working separate time series of composite annual means and quarterly means (Table 1) of the monthly data points in each data series.

The proposed mechanism being tested, i.e., the 'greenhouse gas' effect of water atmospheric vapor on the spatial pattern of temperature in the lower atmosphere, would actually mechanistically act on a synoptic time scale that is much shorter than the annual increments represented in the data series. Moreover, we can conceive of no logical mechanism of a sort that would mechanistically act on a longer time scale that could account for the conundrum of opposite phased variability in the strength of the two interconnected air flows, the trade winds (represented by the SOI) and the upwelling-favorable wind off Peru that feeds directly into them. For example, the climate model results of Garreaud & Falvey (2009) predict trade wind increases that are in the same sense as those of the South American coastal winds rather than the actual data-based opposite-phased ENSO scale variability presented in Fig. 1. Accordingly, successive annual increments even of longer-period 'slow' variations would, from this point

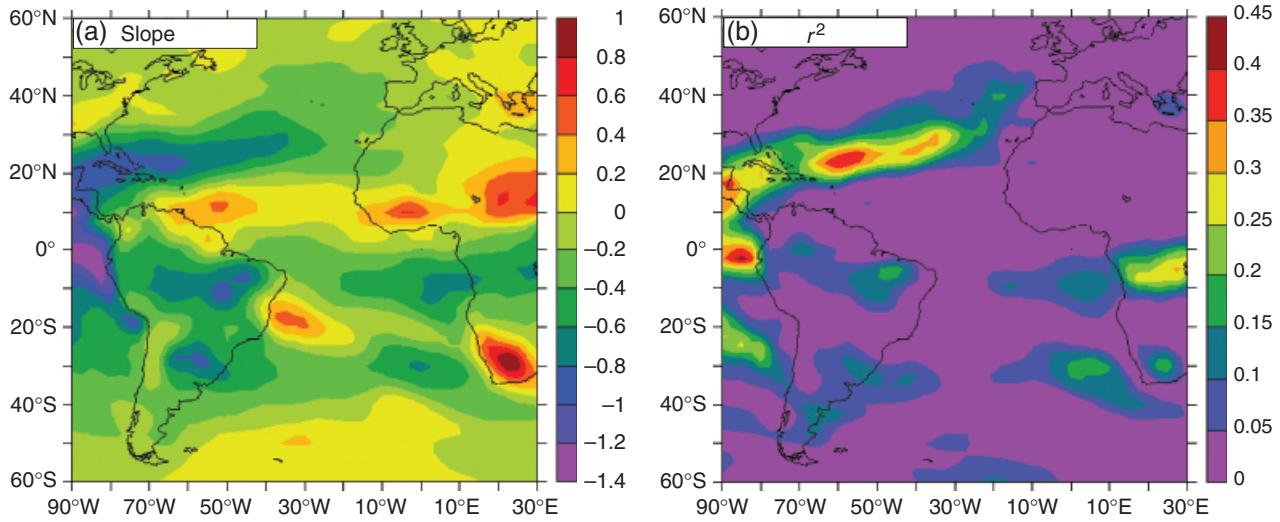

Fig. 4 Distribution of the (a) slopes and (b) '*r*-squared' values of linear regressions, produced in the same way as for Fig. 3, between time series of October through March means of the Southern Oscillation Index and corresponding time series of 'precipitable water' (atmospheric water vapor content) from the National Centre for Environmental Prediction reanalysis data files.

of view, validly represent independent data points with respect to the particular mechanism being addressed in the tests. We indicate the significance levels based on this viewpoint (i.e., assuming each annual data point of each series to represent a separate empirical degree of freedom) by asterisk symbols in Table 1.

However, from the point of view of pure statistics (i.e., that would regard the linkage mechanism as unknown and potentially operating mechanistically on the longer time scales represented in the longer-period 'slow' variations in the annual data series) an assumption of independent annual degrees of freedom might be considered overly optimistic. Accordingly, in order to provide a minimal 'floor' estimate of available degrees of freedom from this standpoint, we have counted crossings of the mean in each data series (Table 2), and then recomputed significance levels based on these reduced estimates ('&' symbols in Table 1). Moreover, to remove the component of autocorrelation directly due to ENSO variability, we have produced a set of series (denoted by 'Δ' prefixes in the names listed in the leftmost columns of Tables 1 and 2) of residuals of the raw series after removing the contribution predicted by a linear regression of the raw series against the SOI series. Finally, we have formed sets of first difference series of the various 'raw' series in order to remove linear trends and suppress long-period variability, thereby increasing the degrees of freedom estimate, represented by crossings of the mean, in the various data series (Table 2).

For our analysis, a time series of atmospheric water vapor concentration that might characterize the variation in associated greenhouse effect is a crucial component. Humidity measured near the sea surface must largely reflect the underlying sea temperature, and thus will not be sufficiently representative of the entire air column thickness over which the water vapor-associated greenhouse effect will operate. For weather analysis purposes, the total precipitable water content of the air column is an important diagnostic quantity that is routinely produced and archived. Long time series of this quantity have been produced on a global basis and made available by two available reanalysis projects undertaken by two different highly competent institutional efforts, the NCEP reanalysis of 'precipitable water vapor' data from 1948 onwards via a joint effort of the U.S. National Center for Environmental Prediction (NCEP, formerly NMC) and the National Center for Atmospheric Research (NCAR), and the ECMWF reanalysis of data between 1979 and 1994 by the European Centre for Medium-Range Weather Forecasts.

The particular difficulties of objective analysis near the Peruvian coast, noted above, are certainly exacerbated in the case of air column water vapor by the fact that before the fairly recent establishment of satellite-based water vapor estimation systems, actual observations within the air column must have been exceedingly rare in the region (i.e., consisting of sporadic balloon-borne radiosondes, etc.). For example, Fig. 2 displays smoothed versions of these two available time series of total air column water vapor at a point near the Peruvian coast. One can see that on these low-frequency time scales, the two series estimating essentially the same property do not agree particularly well. However, in the more recent portions of these series, peaks in indicated water vapor content do tend to visually

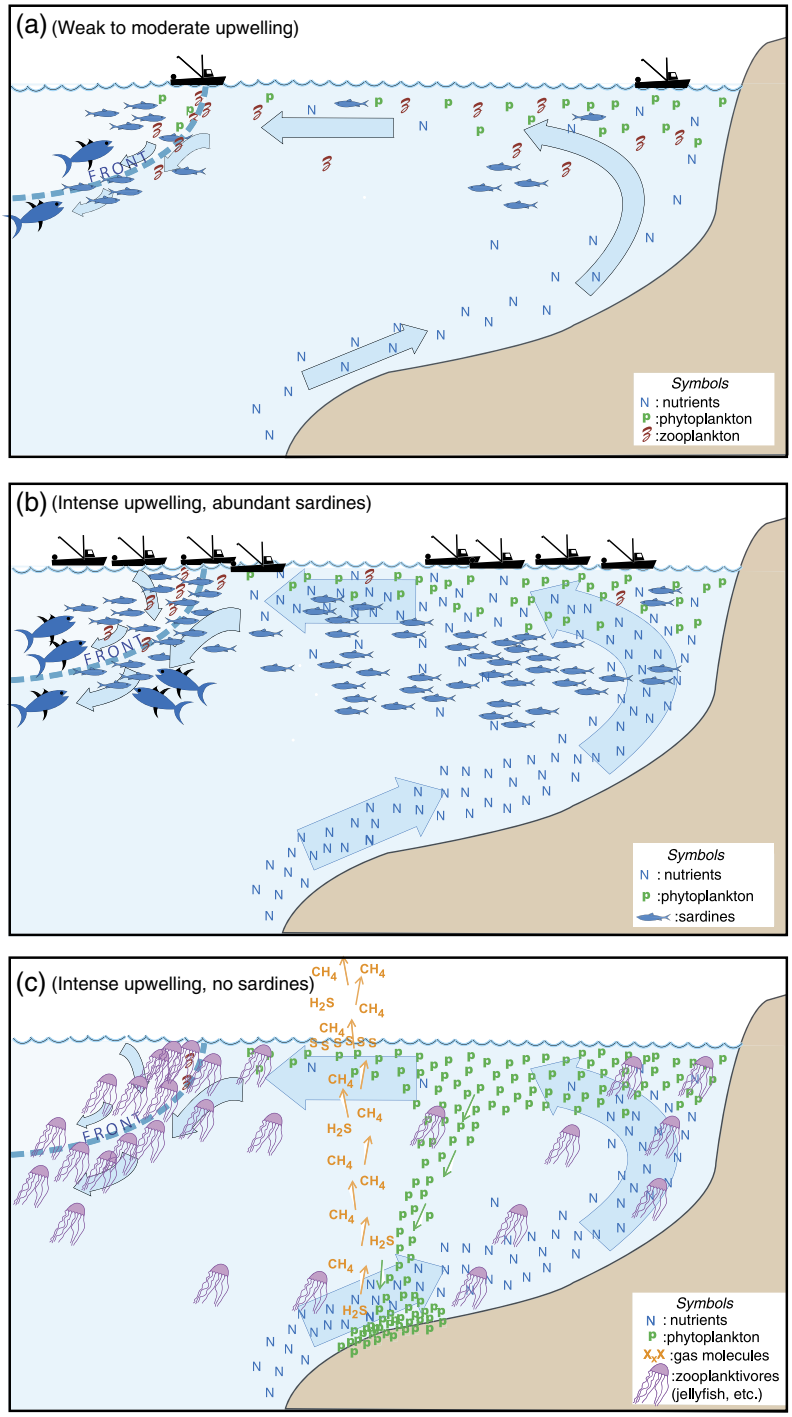

Fig. 5 Schematic diagrams (vertical sections perpendicular to the coast) illustrating: (a) weak to moderate upwelling that allows zooplankton to grow populations to levels sufficient to control growth of phytoplankton production, leading to a conventional local marine food web; (b) intense upwelling that exports zooplankton too rapidly to allow their population growth within the zone, but with abundant strongly swimming sardines able to counter the divergent surface flow to directly consume phytoplankton in the zone, collapsing the local primary production and freeing nutrients to be transported offshore in dissolved form to nourish an enriched conventional food web, and productive fisheries in the wider regional ecosystem; (c) intense upwelling, exporting zooplankton too rapidly to allow their population growth within the zone, leading to unchecked growth of phytoplankton, associated sea floor deposition, and eruptions of noxious, greenhouse-potent gases; concentrated unutilized zooplankton accumulation in offshore upwelling fronts allows breakout of zooplanktivores (medusas, etc.) that may then infest the entire ecosystem.

correspond to El Niño-associated wind increases, particularly in the cases of intense El Niños such as those that occurred in 1982–1983 and in 1997–1998.

Global atmospheric data analysis schemes commonly make use of long-term mean seasonal climatology as a guide to filling in data gaps and to blending data in time and space in physically realistic ways. Such analysis methods may experience problems in portions of the globe that are particularly influenced by ENSO processes, where conditions tend not to vary around a mean state, but rather cluster around two very different opposite extreme states. With respect to our analysis, series of matching annual and quarterly seasonal segments of the two water vapor series (Table 1a) 'explain' respective variances of one another ranging from as low as 11% (4th QTR: October–December) to as high as 56% (second QTR: April–June). The less ENSO-affected seasons clearly exhibit a much higher degree of agreement, which may be somewhat problematic to the present analysis in that we expect water vapor variability to highly responsive to ENSO effects. Even so, during the two most highly ENSO-impacted seasons (the first and fourth quarters that constitute the southern hemisphere's 'heating half of the year'), both available sets of integrated air-column water vapor estimates turn out to be consistently negatively correlated with the SOI, i.e., to the phase of the ENSO cycle on interannual time scales (Table 1b and c), confirming the substantial ENSO control on local atmospheric water vapor content (Quinn *et al*., 1978) evident in Fig. 3d and e. Moreover, the lack of general decline in the correlation when the underlying annual mean series have been previously differenced (Hamilton, 1994) indicates that the relationship is not substantially controlled by long-term trends in the data sets even despite an obvious increasing secular trend in the *Peru–τ*-series (Fig. 2).

Implied linkages

With respect to the seemingly paradoxical out-of-phase relationship between the SOI and the upwelling-favorable wind stress (*Peru–*$\vec{\tau}$) (Table 1d), the indicated correlations tend to be even slightly higher than those between the SOI and either water vapor series. This might be simply a reflection of the imperfections in the water vapor series manifested in their less than impressive mutual intercorrelation and the fact that both the SOI or wind stress series reflect simple summaries of local observations rather being results of sophisticated gap-filling, data-blending analysis schemes that may not be specifically designed for ENSO-dominated situations. In this case, the seasonality of the correlations between series of seasonal segments of the two series (Table 1d) further supports the implication of an essential 'ENSO connection.' The austral spring–summer (fourth QTR–first QTR) 'heating portion of the year' in the southern hemisphere, during which ENSO effects are typically strongest, exhibits highly significant correlations; correlation between these two series drops precipitously in the opposite part of the year during which the Pacific basin-scale ENSO system typically operates much less actively.

But most interestingly, the annual and seasonal correlations of the two water vapor series with corresponding variations in upwelling-favorable wind stress (*Peru–τ*) (Table 1e and f), tend actually to be higher than their correlations with the SOI itself (Table 1b and c), suggesting direct causality (i.e., direct driving of the wind stress variations by the local water vapor content) rather than mere covariation with basin-scale ENSO effects. Indeed, the water-vapor-based 'greenhouse gas' linkage (diagramed in Fig. 1) provides a physical mechanism for the covariation. Moreover, the significant correlations in this case extend to the less ENSO-affected 'cooling half of the year' (second and third QTRs) indicating that water vapor variations other than those directly linked with ENSO may likewise modulate wind stress via this mechanism. In fact, the correlations are highest during the non-ENSO-affected portion of the year, perhaps reflecting the better reliability of the water vapor series during those seasons.

It is important to note that in the cases of the SOI and the wind stress the various quarterly series are strictly independent of one another, sharing no data at all, and in the cases of the each of the two water vapor series are essentially so, transferring information for no more than a day or so at the intersection of different quarters depending on the analysis procedure used. Accordingly, a most impressive aspect of Table 1 is that all the correlations between all the corresponding variables, whether individually statistically significant or not, are without a single exception in the correct directional sense (i.e., of the correct sign) to conform to the set of mechanistic linkages proposed herein. This holds regardless of season, indicating the essential causal relationship extends beyond the ENSO-dominated seasons, and in spite of the fairly poor levels of agreement between the two available time series of estimates of the proposed causative variable, water vapor. To quantify the statistical significance of this consistent agreement, we multiply the four calculated seasonal probability levels together so as to estimate the likelihood of reaching a similar repeated correlation among random independent data series for four different independent quarterly seasonal segments that possess the same conservatively estimated degrees of freedom represented by the least number of crossings of the mean (Table 2) among each series pair (corresponding to the

'&' criteria represented in Table 1). The calculated results are impressive, whether for the 'raw' data series, the 'Δ' series that have had the ENSO-correlated component removed, or the first-differenced series in which effects of trends and other longer-term variations are suppressed. In the case of the tests of the wind stress series against the NCEP water vapor series, the composite probabilities are all <0.001, while against the EMRFC series they are all less than an even more impressive 0.0001.

To summarize, the opposite-phased ENSO-scale variations in the upwelling-favorable wind off Peru and the Pacific trade winds (SOI) seem to be well rationalized as resulting from variations in greenhouse gas content within the thermal low-pressure cell that forms over the Peruvian landmass. Moreover, even when the ENSO-correlated components of the various series are removed, the non-ENSO-correlated residuals (the respective 'Δ'series) remain highly correlated (Table 1e and f). Accordingly, we argue that the results reported here can be viewed as a successful proxy test of the longstanding hypothesis (Bakun, 1990, 1992) that enhanced concentrations of atmospheric greenhouse gases can lead to intensification of the upwelling-favorable winds that drive the major coastal upwelling ecosystems of the world's oceans (Fig. 1). Also, it may be worth reiterating that for this proxy test, the sequence of ENSO-scale and other variations has offered a wealth of empirical realizations of the process, rather than the mere secular trend that is ordinarily all that is available for empirically addressing the effect of the longer-term industrial-age buildup of atmospheric greenhouse gases.

It should be said that these results, as strong as they seem to be, do not exclude the likelihood that Enfield's (1981) mechanism cloudiness also may be contributing to the out-of-phase variability of the SOI and the upwelling-favorable wind off Peru that is evident in Fig. 2. However, Warner (2004) states that coastal stratus is generally absent during austral summer season when El Niño effects are more pronounced and when the correlation between the two tend to be higher (Table 1d), austral winter being the season in which coastal stratus clouds tend to prevail. Warner also states that Peruvian coastal stratus extends only to the slopes of the near-coastal mountain range, whereas in the large expanse of desert to the east of the coastal range, the sky remains clear. Thus the cloudiness effect would seem to act over a considerably smaller scale than would the greenhouse-related effect of water vapor enhancement, and less strongly during the seasons that seem to control the oppositely phased interannual variation in equatorial trade winds and upwelling-favorable winds off Peru that is highlighted in Fig. 2.

To the extent that the results are reflective of the greenhouse gas effect of atmospheric water vapor variations in coastal thermal low-pressure cells, they indeed would appear to support the prognosis for increased intensity of upwelling-favorable winds in the major coastal upwelling zones of the world's oceans, and in fact in any extra-tropical coastal ocean region characterized by thermal low-pressure cell development on the adjacent continental coastland. Enfield's cloudiness mechanism would, to the extent it were acting in any particular regional case, likely reinforce increases in upwelling in that an intensified band of cool upwelled water near the coast appears to generally to reduce coastal cloudiness (Trewartha, 1961; Hsu, 1988; Bakun, 1990).

Apparent SE Atlantic exception

A possible 'exception that proves the rule' example is offered by the Benguela upwelling system off southwestern Africa where, in contrast to the reported increasing trends seen in the Peru, California, and Canary systems (Bakun, 1990, 1992; Roy & Reason, 2001; Vargas *et al.*, 2007) an apparent recent decline in upwelling intensity is reported (Peard, 2007). In this case, the multiple realizations offered by repeating ENSO cycles make it possible to surmise empirically (Fig. 4) that water vapor content over the landmass in the Benguela region varies in substantial relation to (i.e., sizeable amplitude of the indicated effect coincides with satisfactory statistical significance), but directly out of phase with, that of the eastern Pacific. Thus, as the Pacific basin becomes progressively more 'El Niño'-like as climate change proceeds (Vecchi *et al.*, 2006), the Benguela coastlands might be expected to become less humid. Because, water vapor is the most important atmospheric greenhouse gas, the reduced greenhouse effect could overbalance the local effects of the buildup of carbon dioxide, methane and other anthropogenic greenhouse gases with the result that the coastal thermal low-pressure cell would relax rather than intensify. (Note that in Fig. 4 another zone of implied substantial linkage of water vapor content to ENSO, but in the opposite sense, also exists offshore; to the extent that this could signify a tendency for lowered atmospheric pressure offshore this could imply an even further weakening of the upwelling-favorable coastwise wind tendency.) Accordingly, the locally wind-induced upwelling in the Benguela region could tend to weaken rather than intensify, offering a potential explanation for the current weakening trend in upwelling-favorable winds in that particular region and a logical basis to consider whether this region may in fact continue to run counter to the expected climate change-associated global trend (depending on which greenhouse effect turns

out to be stronger, that due to local anthropogenic greenhouse gas buildup or that related to remotely teleconnected ENSO-associated alterations in local atmospheric water vapor tendencies). Of course, observed trends in different regions may also be affected by decadal- to centennial-scale climate variability, rather than trends associated with the accumulation of anthropogenic greenhouse gasses.

Ecological implications

In any case, it is far from clear that intensified upwelling would necessarily be favorable for fish production and other valued ecosystem characteristics. There are a large number of different processes that could affect the transfer of increasing wind to increasing productivity, which include nutrient concentrations of source waters, regional changes in stratification and/or thermocline structure, and basin-scale changes in thermocline structure, to name just a few. Off Peru, and probably also off California, the projected decline in the Pacific near-equatorial trade wind circulation (Vecchi *et al*., 2006) should, on average, impart a more El Niño-like character to the subsurface source waters. This might well counteract the nutrient-enrichment effects of enhanced upward transfer rates. Indeed, Brady *et al*. (2002) report that a given wind stress anomaly produces a weaker SST anomaly in their enhanced-CO2 climate model simulations off Peru, implying also less vigorous upward nutrient transfers to support primary production. On the other hand, with decreased strength of the trade wind circulation, less extreme individual El Niño episodes might be anticipated, as has indeed been suggested in model simulation results (Otto-Bliesner *et al*., 2003). Less extreme episodes might help management efforts to avoid short-term El Niño-related fish stock collapses. However, it has been hypothesized that, on the slightly longer term, intense El Ninos may be required to periodically reinitiate the sequences of highly productive transient biological population responses that underlie that system's remarkable fishery production (Bakun & Weeks, 2008). In contrast, the essentially more productive, but much less intensely perturbed, Canary and Benguela upwelling systems typically yield less than one-twentieth of the annual fishery harvest of the weaker, less productive Peru system (Carr, 2001). Thus the projected decline in the Pacific equatorial trade winds, in presaging weaker El Niño episodes, could have long-term adverse impacts on the fishery productivity of the Peru marine ecosystem even though the local upwelling rate may actually increase rather than decrease.

In general, therefore, even if the projection for increases in upwelling favorable winds is entirely correct, ramifications in terms of future trends in upwelling-based transfers of plant nutrients to support primary production are somewhat muddled, particularly in the case of the Pacific Ocean systems where source water issues and/or changes in thermocline structure might be overriding considerations. However, there are other extremely important ecological implications that depend directly on the upwelling-associated offshore surface transport, and thus are largely independent of issues of source water origin or character. We focus on just these implications here.

For example, in a normal situation of moderate upwelling (Fig. 5a), upwelled nutrients support a productive *in situ* food web wherein photosynthesizing phytoplankton nourish a flourishing zooplankton community. In the process, the growing phytoplankton and zooplankton concentrations are transported offshore toward a convergent frontal system where the more dense upwelling-conditioned surface water meets and sinks beneath less dense oceanic surface waters (Sverdrup, 1938; Barth, 1989; Marañón & Fernández, 1995). Here, planktonic organisms that are able to maintain a preferred depth level become highly concentrated as the waters in which they are entrained converge horizontally and sink vertically through that level. This concentrated food source attracts small pelagic fishes and other plantivorous nekton, which in turn attract larger pelagic predators as well as fishing operations that may employ modern means such as satellite imagery to locate the advantageous frontal interfaces.

But with increased upwelling rate, the difference in typical generation times between phytoplankton and zooplankton may result in flushing the herbivorous zooplankton, that normally would exert controls on phytoplankton growth, from the upwelling zone (Bakun & Weeks, 2004). In such a situation, which features an excess of upwelled nutrients, the rapidly multiplying phytoplankton may grow unrestrainedly in abundance. In situations where a large population of phytoplankton-consuming nekton (e.g., sardines) may be operating, these may counter the increased offshore transport by their own swimming power and substantially assume the role of the absent herbivorous zooplankton in consuming excess phytoplankton production within the upwelling zone. In such a case, the increasing supply of upwelled and recycled nutrients may support a greatly enriched trophic system (Fig. 5b) that, in addition to supporting very productive fisheries, serves to keep upwelled nutrients in the system rather than being trapped and sedimented within the upwelling zone (Fig. 5c), where they may contribute to severe, not easily reversible changes in ecosystem function (e.g., hypoxia, toxic gas eruptions, red tides, etc.).

However, as the rate of offshore transport continues to increase, particularly if the available small pelagic omnivorous fish may be subject to overly heavy fishing, various factors may combine to cause an abrupt ecosystem *regime shift* (Fig. 5c). For example, increasing sedimentation of unconsumed phytoplankton production onto the floor of the continental shelf may result in sea floor hypoxia and release of noxious products of anaerobic decomposition that include poisonous hydrogen sulfide and greenhouse-active methane. Increased transport of plankton into the offshore fronts may result in explosive breakouts of less mobile zooplanktivores such as jellyfish that may initially be retained within the fronts, but upon establishing critical mass may break out to infest the entire system where they may voraciously consume the eggs and larvae of fish (Arai, 1997) that may have earlier acted to constrain them through competition or predation (Richardson *et al*., 2009). Notably, jellyfish also seem particularly well equipped to deal with associated hypoxic conditions in the water column (Purcell *et al*., 2001; Decker, 2004) that may accompany such a shift.

The upwelling zone located near Lüderitz, Namibia, which is recognized as the world's most intense eastern ocean upwelling zone, may represent a 'poster child' for potential changes (Bakun & Weeks, 2006). The Namibian sardine resource was decimated by massive overfishing several decades ago and has never substantially recovered. Subsequently, the entire large marine ecosystem seems to have been burdened by a heavy infestation of jellyfish (Lynam *et al*., 2006). Meanwhile toxic red tide blooms continue to occur, while eruptions of toxic gases, leaving sea surface signatures as large as the state of New Jersey, strip dissolved oxygen from the water column, inflict noxious smells and caustic rain on the adjacent coastlands, and cause episodic kills of fish and other organisms (Weeks *et al*., 2004).

Certain 'echoes' of this situation are becoming evident in other regions. Repeated annual hypoxic 'dead zones' have been a recent development in the upwelling zone off Oregon (Chan *et al*., 2008). Meanwhile, widespread marine hypoxia (Diaz & Rosenberg, 2008), toxic red tides (Pitcher & Nelson, 2006; Ryan *et al*., 2009), and jellyfish infestations (Mills, 2001; Richardson *et al*., 2009) appear to represent increasingly unwelcome trends in many marine ecosystems of the world's oceans. Thus, whatever the actual effect on the primary productivity of these most productive of the world's regional marine ecosystems, the theorized climate change-related increases in upwelling-favorable winds in upwelling ecosystems discussed here would seem by and large to add momentum to these other unwelcome trends.

One available mitigation action, separate from dealing with the ultimate greenhouse gas issues themselves, would seem to be careful avoidance of destructive overfishing of small filter-feeding fishes, such as sardines, that are reasonably considered to be more or less effective in countering eutrophication, red tides and hypoxia (Bakun & Weeks, 2004; Irigoien *et al*., 2005; Vasas *et al*., 2007; Chan *et al*., 2008) and jellyfish explosions (Daskalov, 2002; Bakun & Weeks, 2006; Richardson *et al*., 2009).

References

Arai MN (1997) *A Functional Biology of Scyphozoa*. Chapman & Hall, New York.

Bakun A (1990) Global climate change and intensification of coastal ocean upwelling. *Science*, **247**, 198–201.

Bakun A (1992) Global greenhouse effects, multi-decadal wind trends and potential impacts on coastal pelagic fish populations. *ICES Marine Science Symposia*, **195**, 316–325.

Bakun A, Weeks SJ (2004) Greenhouse gas buildup, sardines, submarine eruptions, and the possibility of abrupt degradation of intense marine upwelling ecosystems. *Ecology Letters*, **7**, 1015–1023.

Bakun A, Weeks SJ (2006) Adverse feedback sequences in exploited marine ecosystems: are deliberate interruptive actions warranted? *Fish and Fisheries*, **7**, 316–333.

Bakun A, Weeks SJ (2008) The marine ecosystem off Peru: what are the secrets of its shery productivity and what might its future hold? *Progress in Oceanography*, **79**, 290–299.

Barth JA (1989) Stability of a coastal upwelling front 2. Model results and comparison with observations. *Journal of Geophysical Research*, **94** (C8), 10,857–10,883.

Bigg GR (1988) Sea level and meridional wind trends along the South American coast. *Tropical Ocean-Atmosphere Newsletter*, **43**, 1–2.

Bigg GR, Gill AE (1986) The annual cycle of sea level in the eastern tropical Pacific. *Journal of Physical Oceanography*, **16**, 1055–1061.

Bjerknes J (1966) A possible response of the atmospheric Hadley circulation to equatorial anomalies of ocean temperature. *Tellus*, **18**, 820–829.

Boville BA, Gent PR (1998) The NCAR climate system model, version one. *Journal of Climate*, **11**, 1115–1130.

Brady EC, Otto-Bliesner BL, Shields C (2002) *ENSO response to increased greenhouse gas forcing in the NCAR climate system model*. American Geophysical Union, Fall Meeting 2002. Abstract #PP61A-0292.

Cane MA, Clement AC, Kaplan A, Kushnir Y, Pozdnyakov D, Seager R, Zebiak SE, Murtugudde R (1997) Twentieth-century sea surface temperature trends. *Science*, **275**, 957–960.

Cardone VJ, Greenwood JG, Cane MA (1990) On trends in historical wind data. *Journal of Climate*, **3**, 113–127.

Carr ME (2001) Estimation of potential productivity in eastern boundary currents using remote sensing. *Deep-Sea Research II*, **49**, 59–80.

Chan F, Barth JA, Lubchenco J, Kirinich A, Weeks H, Peterson WT, Menge BA (2008) Emergence of anoxia in the California current large marine ecosystem. *Science*, **319**, 920.

Csanady GT (1978) The arrested topographic wave. *Journal of Physical Oceanography*, **8**, 47–62.

Daskalov GM (2002) Overfishing drives a trophic cascade in the Black Sea. *Marine Ecology Progress Series*, **225**, 53–63.

Decker MB, Breitburg DL, Purcell JE (2004) Effects of low dissolved oxygen on zooplankton predation by the ctenophore *Mnemiopsis leidyi*. *Marine Ecology Progress Series*, **280**, 163–172.

Diaz RJ, Rosenberg R (2008) Spreading dead zones and consequences for marine ecosystems. *Science*, **321**, 926–929.

Diffenbaugh NS, Snyder MA, Sloan LC (2004) Could CO_2-induced land-cover feedbacks alter near-shore upwelling regimes? *Proceedings of the National Academy of Sciences US*, **101**, 27–32.

Di Lorenzo E, Miller AJ, Schneider N, McWilliams JC (2005) The warming of the California current: dynamics and ecosystem implications. *Journal of Physical Oceanography*, **35**, 336–362.

Enfield DB (1981) Thermally driven wind variability in the planetary boundary layer above Lima, Peru. *Journal of Geophysical Research*, **86**, 2005–2116.

Enfield DB, Allen JS (1980) On the structure and dynamics of monthly mean sea level anomalies along the Pacific coast of North and South America. *Journal of Physical Oceanography*, **10**, 557–578.

Gandin LS (1965) *Objective Analysis of Meteorological Fields*. Israel Program for Scientific Translations, Jerusalem.

Garreaud RD, Falvey M (2009) The coastal winds off western subtropical South America in future climate scenarios. *International Journal of Climatology*, **29**, 543–554.

Gutiérrez D, Sifeddine A, Field DB *et al*. (2009) Rapid reorganization in ocean biogeochemistry off Peru towards the end of the little ice age. *Biogeosciences*, **6**, 835–848.

Hamilton JD (1994) *Time Series Analysis*. Princeton University Press, Princeton, NJ.

Houghton JT (2001) *IPCC Report*. Cambridge University Press, Cambridge, UK.

Hsieh WW, Boer GJ (1992) Global climate change and ocean upwelling. *Fisheries Oceanography*, **1**, 333–338.

Hsu S-A (1988) *Coastal Meteorology*. Academic Press, San Diego, CA, USA, ISBN 0123579554, 9780123579553, 260 pp.

Irigoien X, Flynn KJ, Harris RP (2005) Phytoplankton blooms: a 'loophole' in microzooplankton grazing impact? *Journal of Plankton Research*, **27**, 313–321.

Ludwig FL, Sinton D (2000) Evaluating an objective wind analysis technique with a long record of routinely collected data. *Journal of Applied Meteorology*, **39**, 335–348.

Lynam CP, Gibbons MJ, Axelsen BJ, Sparks CAJ, Coetzee J, Heyward BJ, Bierly SS (2006) Jellyfish overtake fish in a heavily fished ecosystem. *Current Biology*, **16** (13), R492–R493.

Manabe S, Weatherald RT (1980) On the distribution of climate change resulting from an increase in CO_2 content of the atmosphere. *Journal of Atmospheric Science*, **37**, 99–118.

Marañón E, Fernández E (1995) Changes in phytoplankton ecophysiology across a coastal upwelling front. *Journal of Plankton Research*, **17**, 1999–2008.

Mendelssohn R, Schwing FB (2002) Common and uncommon trends in SST and wind stress in the California and Peru–Chile current systems. *Progress in Oceanography*, **53**, 141–162.

McGregor HV, Dima M, Fischer HW, Mulitza S (2007) Rapid 20th-century increase in coastal upwelling off northwest Africa. *Science*, **315**, 637–639.

Mills CE (2001) Jellyfish blooms: are populations increasing globally in response to changing ocean conditions? *Hydrobiologia*, **451**, 55–68.

Mote PW, Mantua NJ (2002) Coastal upwelling in a warmer future. *Geophysical Research Letters*, **29**, 2138–2141.

Otto-Bliesner BL, Brady EC, Shin S-I, Liu Z, Shields C (2003) Modeling El Niño and its tropical teleconnections during the last glacial–interglacial cycle. *Geophysical Research Letters*, **30**, 2198.

Paulik GJ (1971) Anchovies, birds, and fishermen in the Peru current. In: *Environment: Resources, Pollution and Society* (ed Murdoch WW), pp. 156–185. Sinauer Associates, Stanford, CT, USA.

Peard KR (2007) *Seasonal and interannual variability of wind-driven upwelling at Lüderitz, Namibia*. MSc Thesis, University of Cape Town, South Africa.

Pitcher GC, Nelson G (2006) Characteristics of the surface boundary layer important to the development of red tide on the southern Namaqua shelf of the Benguela upwelling system. *Limnology and Oceanography*, **51**, 2660–2674.

Purcell JE, Breitburg DL, Decker MB, Graham WM, Youngbluth MJ, Raskoff KA (2001) Pelagic cnidarians and ctenophores in low dissolved oxygen environments. In: *Coastal Hypoxia: Consequences for Living Resources and Ecosystems*. *Coastal and Estuarine Studies 58* (eds Rabalais NN, Turner RE), pp. 77–100. American Geophysical Union, Washington, DC.

Quinn WH, Zopf DD, Short KS, Kuo Yang TRW (1978) Historical trends and statistics of the Southern Oscillation – El Niño and Indonesian droughts. *Fisheries Bulletin, US*, **76**, 663–678.

Ramage CS (1987) Secular change in reported wind speeds over the ocean. *Journal of Climate and Applied Meteorology*, **26**, 525–528.

Richardson AJ, Bakun A, Hays GC, Gibbons MJ (2009) The jellyfish joyride: causes, consequences and management responses to a more gelatinous future. *Trends in Ecology & Evolution*, **24**, 312–322. (Corrected proof, Available online 25 March 2009).

Rockel B, Castro CL, Pielke RA Sr, von Storch H, Leoncini G (2008) Dynamical downscaling: assessment of model system dependent retained and added variability for two different regional climate models. *Journal of Geophysical Research*, **113**, D21107, doi: 10.1029/2007JD009461.

Roy C, Reason C (2001) ENSO-related modulation of coastal upwelling in the eastern Atlantic. *Progress in Oceanography*, **49**, 245–255.

Ryan JP, Fischer AM, Kudela RM, Gower JFR, King SA, Marin R III, Chavez FP (2009) Inuences of upwelling and downwelling winds on red tide bloom dynamics in Monterey Bay, California. *Continental Shelf Research*, **29**, 785–795.

Santos AMP, Kazmin AS, Peliz Á (2005) Decadal changes in the Canary upwelling system as revealed by satellite observations: their impact on productivity. *Journal of Marine Research*, **63**, 359–379.

Schwing FB, Mendelssohn R (1997) Increased coastal upwelling in the California current system. *Journal of Geophysical Research*, **102**, 3421–3438.

Shannon V, Crawford RJM, Pollock DE *et al*. (1992) The 1980s – a decade of change in the Benguela ecosystem. In: *Benguela Trophic Functioning* (eds Payne AIL, Brink KH, Mann KH, Hilborn R), *South African Journal of Marine Science*, **12**, 271–296.

Snyder MA, Sloan LC, Diffenbaugh NS, Bell JL (2003) Future climate change and upwelling in the California current. *Geophysical Research Letters*, **30**, 1823, doi: 10.1029/2003GL017647.

Sverdrup HU (1938) On the process of upwelling. *Journal of Marine Research*, **1**, 115–164.

Trewartha GT (1961) *The Earth's Problem Climates*. University of Wisconsin Press, Madison.

UCSD. (2008) Stronger coastal winds due to climate change may have far-reaching effects. University of California – Santa Cruz (December 22, 2008). *Science Daily*. Available at http://www.sciencedaily.com–/releases/2008/12/081219172037.htm (accessed March 17, 2009).

Van Geen A, Luoma SN, Fuller CC, Anima R, Clifton HE, Trumbore S (1992) Evidence from Cd/Ca ratios in foraminifera for greater upwelling off California 4,000 years ago. *Nature*, **358**, 54–56.

Vargas G, Pantoja S, Rutllant JA, Lange CB, Ortlieb L (2007) Enhancement of coastal upwelling and interdecadal ENSO-like variability in the Peru–Chile Current since late 19th century. *Geophysical Research Letters*, **34**, L13607, doi: 10.1029/2006GL028812.

Vasas V, Lancelot C, Rousseau V, Jordán F (2007) Eutrophication and overfishing in temperate nearshore pelagic food webs: a network perspective. *Marine Ecology Progress Series*, **336**, 1–14.

Vecchi GA, Soden BJ, Wittenberg A, Held IM, Leetma A, Harrison MJ (2006) Weakening of tropical Pacific atmospheric circulation due to anthropogenic forcing. *Nature*, **425**, 73–76.

von Storch H, Hewitson B, Mearns L (2000) Review of empirical downscaling techniques. In: *Regional Climate Development Under Global Warming, General Technical Report 4* (eds Iversen T, Høiskar BAK), NILU,

Kjeller, Norway. Available at http://regclim.met.no/rapport_4/presentation02/presentation02.htm (accessed April 18, 2009).

Yelland M, Taylor PK (1996) Wind stress measurements from the open ocean. *Journal of Physical Oceanography*, **26**, 541–558.

Wang M, Dykes DW, Book JW (2009) Climate projections for selected large marine ecosystems. *Journal of Marine Systems*, doi: 10.1016/j.jmarsys.2008.11.028.

Warner TT (2004) *Desert Meteorology*. Cambridge University Press, Cambridge, UK, ISBN 0521817986, 9780521817981. 595 pp.

Weeks SJ, Currie B, Bakun A, Peard KR (2004) Hydrogen sulphide eruptions in the Atlantic Ocean off southern Africa: implications of a new view based on SeaWiFS satellite imagery. *Deep-Sea Research I*, **51**, 153–172.

Wooster WS, Reid JL (1963) Eastern boundary currents. In: *The Sea*, Vol. 2 (ed. Hill MN), pp. 253–280. Interscience Publications, New York.

Wyrtki K (1975) El Niño – the dynamic response of the equatorial Pacific. *Journal of Physical Oceanography*, **5**, 572–584.